Supporting Information

Hughes et al. 10.1073/pnas.1108617109

SI Materials and Methods

Synthesis of *N*-[3-[(4-benzoylphenyl)formamido]propyl] methacrylamide (BPMAC). BPMAC ($C_{21}H_{22}N_2O_3$, 350.2 g mol^{-1}) monomer was synthesized via reaction of the succinimidyl ester of 4-benzoylbenzoic acid (323.3 g mol^{-1}; B1577; Invitrogen) with *N*-(3-aminopropyl)methacrylamide hydrochloride (APMA, 178.7 g mol^{-1}; 21200; Polysciences) in the presence of catalytic triethylamine (TEA) in dimethylformamide (DMF). A mixture of the reactants and TEA at 50 mM each in DMF was incubated overnight (18 h) at room temperature, centrifuged at 18,000 × *g* for 5 min, and the pellet discarded. The supernatant was incubated on a tube inverter for 24 h with 30 mg isothiocyanate-functionalized (primary amine-reactive) polystyrene beads (538604; Sigma) for every 100 μmol of APMA initially added to the reaction. The mixture was then spun at 18,000 × *g* for 5 min and the supernatant passed through a 0.2-μm syringe filter. A 10-fold excess of acetone was added to the filtrate and the mixture dried in vacuo. The BPMAC product (white powder) was verified by ^{1}H NMR [400 MHz, d_6-DMSO, δ 8.79 (t, 1H), 8.04 (t, 1H), 8.02 (d, 2H), 7.80 (d, 2H), 7.75 (d, 2H), 7.70 (t, 1H), 7.58 (t, 2H), 5.67 (s, 1H), 5.32 (s, 1H), 3.31 (q, 2H), 3.18 (q, 2H), 1.86 (s, 3H), 1.71 (quin, 2H)] and mass spectrometry (electrospray ionization, m/z 351.2, $C_{21}H_{22}O_3N_2 + H^+$). The abbreviations s, d, t, and q signify singlet, doublet, triplet, and quartet, respectively. Stocks of BPMAC at 100 mM in DMSO were stored at −20 °C until use, and were stable for at least 12 mo.

Purified Proteins and Antibodies. Pharmalyte 3–10 was minimally labeled by mixing a 1% solution in 200 mM sodium bicarbonate pH 8.3 with an equal volume of 2.27 mM CE540 in DMSO (346.5 g mol^{-1}, 15102; Active Motif; dye:ampholyte ratio of *ca.* 0.1 given average ampholyte MW of *ca.* 500 g mol^{-1}; ref. 1) and incubating at 50 °C for 1 h. WT GFP (recombinant from *Escherichia coli*, *Aequoria victoria* wild-type; 632373; Clontech), purified prostate specific antigen (PSA) (from human seminal fluid; ab78528; Abcam), and the Serva isoelectric focusing (IEF) 3–10 protein marker mix (39212-01; Invitrogen) were labeled with CE540 according to manufacturer instructions. 1° antibodies to PSA (goat pAb; AF1344; R&D Systems; mouse mAb; M167; CalBioreagents) were labeled with Alexa Fluor 568 dye according to manufacturer instructions (Invitrogen). Fluorophore:protein molar labeling ratios (MR) were 4.0 and 4.7 for the pAb* and mAb* respectively. The rabbit anti-goat IgG 2° was labeled similarly (MR = 3.2; 305-005-045; Jackson ImmunoResearch). The 1° goat pAb to GFP was prelabeled with Texas red by the manufacturer (MR = 2.9; ab6660; Abcam). Fluorescently labeled proteins were purified using P-6 (PSA, GFP) or P-30 (antibodies) Bio-Spin chromatography columns (Bio-Rad) to remove free dye prior to loading on light-activated volume-accessible gels (LAVAgels).

Buffers. Sample loading buffer was of the same composition as gel precursor, but lacked monomers and initiators. Catholyte was 20 mM lysine, 20 mM arginine pH 10.1. Anolyte was 70 mM phosphoric acid. pH gradient washout buffer/probing buffer was 15 mM glycine pH 9.9, 3% CHAPS, 200 mM nondetergent sulfobetaine (NDSB) 256, 10% sorbitol.

Microscopy and UV Exposure. Chip imaging was conducted using an Olympus IX50 inverted fluorescence microscope equipped with CCD camera (CoolSNAP HQ^2; Photometrics) motorized stage (Applied Scientific Instrumentation) and shutter systems (Sutter Instrument) controlled by MetaMorph software (Molecular Devices). Flood UV duty was provided by a Hamamatsu Lightningcure LC5 directed through a Lumatec series 380 liquid light guide with inline UV filter (300–380 nm bandpass; XF1001; Omega Optical) suspended approximately 10 mm above the chip plane with UV power at chip plane of 160 mW cm^{-2} (UV513AB meter; General Tools). Kinetic study of LAVAgel immobilization was conducted via spot UV exposure through a 10x objective (Olympus UPlanFl, N.A. 0.3) and XF1001 exciter, with UV power at the chip plane of 40 mW cm^{-2}.

Green and red fluorescence channels were imaged at 10x using Omega Optical filter cubes optimized for GFP (XF100-3) and DsRed2 (XF111-2). IEF pI markers were imaged prior to UV immobilization using a custom UV-longpass filter cube (excitation 300–380 nm, emission >410 nm; XF1001, XF3097; Omega Optical) and channel positions were manually scored (gradient drift between focused-state marker and analyte imaging steps was assumed to be negligible). Exposure times were 50 ms for prewashout scans and 400 ms postwashout, all with 4 × 4 pixel binning (CCD signals were linear in exposure time). Real-time single-point imaging of GFP isoform dynamics and GFP was conducted in burst acquisition mode to eliminate camera and image transfer lag.

Transformation of fluorescence data via linear fits to pI markers and associated data processing was performed using MATLAB scripts written inhouse (MathWorks). Least-squares fitting of kinetic data was performed using gnuplot software.

LAVAgel Chip Operation Protocol. After gelation, LAVAgel access wells were filled with gel buffer. Samples (30 μL) were made in loading buffer and titrated to pH 9.9 with 1.5 μL 1M NaOH just prior to introduction at loading wells (3 μL per well). Sample injection was performed at 200 V cm^{-1} for 3 min. Catholyte and anolyte buffers were used to wash opposite wells twice; wells were subsequently filled. Focusing was conducted simultaneously for the four devices in each chip (i.e., all well pairs), at 50 V cm^{-1} for 4 min; 100 V cm^{-1}, 5 min; 200 V cm^{-1}, 5 min. Three-minute 300 V cm^{-1} focusing, imaging, and flood UV exposure steps were conducted individually for each device in series. Imaging of pI markers via 50-ms exposures was preceded by any green and/or red channel scans required. Following marker imaging, the chip was moved into position beneath the lightguide tip under motorized stage control. Under stopped electric field, 2 × 5 s flood UV exposures were applied in neighboring spots (*ca.* 5-mm apart along the channel axis) to ensure uniform UV dosage. The final focusing, imaging, and flood exposure steps were repeated for the other devices on the same chip. Refocusing and imaging was conducted as necessary prior to simultaneous washout of all devices. Access wells were washed and filled with glycine washout/probe buffer. Mobilization and washout of pH gradients to the anodic wells was achieved via a 20-min electrophoretic step. Labeled antibody probes were diluted in washout/probe buffer, loaded, and removed from LAVAgels in 20-min electrophoretic steps; wells were washed with buffer as required to prevent undesired cross-reaction of 1° and 2° probes in access wells. Probe loading and washout were conducted in opposite directions to minimize nonspecific signal remaining after washout. Final green and/or red scans were performed as necessary with 400-ms image exposure time.

In the case of kinetic studies of LAVAgel immobilization, GFP was electrophoretically loaded at 200 V cm^{-1} as a homogeneous stream in untitrated loading buffer (pH 6.5). UV exposure dosage applied via the microscope mercury lamp was tightly con-

trolled via the mechanical excitation shutter. Twenty-minute GFP washout was performed by replacing sample with fresh untitrated loading buffer before application of 200 $V\,cm^{-1}$ field in the opposite direction to loading for 20 min.

Removal of the LAVAgel matrix after use was achieved by overnight incubation of the chip in a 2:1 solution of 70% perchloric acid and 30% hydrogen peroxide heated to 75 °C, allowing efficient recycling of glass chips, as previously described (2).

Cell Culture. The human prostate cancer cell lines DU145 and LAPC-4 were obtained from American Type Culture Collection and Dr. Charles Sawyers (University of California, Los Angeles), respectively (3, 4). DU145 cells were grown in DMEM (Invitrogen) and LAPC-4 cells in Iscove's Modified Dulbecco's Medium (Invitrogen) supplemented with 10% FBS (HyClone) and 100 μg/mL of gentamycin (Fisher) in 100-mm dishes at 37 °C in 5% CO_2. Medium was changed twice a week and the cells were subcultured using TrypLE Express (Invitrogen).

Lysate Preparation. One day after feeding, three to five 100-mm dishes of DU145 cells at 90% confluency or LAPC-4 cells at 75% confluency were used to prepare cell lysates. Each dish was washed once with Hepes-buffered saline (HBS) and then incubated with 1 mL of TrypLE Express at 37 °C for 5 min. Dishes were washed with HBS to collect cells, which were then centrifuged to pellet the cells. After the HBS was removed, each cell pellet was resuspended in HNTG buffer (20 mM Hepes pH 7.5, 25 mM NaCl, 0.1% Triton X-100, 10% glycerol). Each of these samples was then supplemented with 1:100 Protease Inhibitor Cocktail (Calbiochem) and 1 mM phenylmethylsulfonyl fluoride (Sigma). Samples were incubated on ice for 30 min, vortexing every 5 min. Next, samples were centrifuged at 16,000 × *g* for 10 min at 4 °C. The lysate supernatant was collected and the protein concentration was measured using a Bio-Rad protein assay (Bio-Rad). Aliquots of 20 μL from each lysate were frozen on dry ice and stored at −80 °C.

Serum Preparation. Pooled negative control serum was from US Biological (S1005-05). Advanced metastatic prostate cancer patient blood samples were collected between 1998 and 1999 with informed consent under an institutional review board-approved protocol in red-top vacutainer tubes (BD Biosciences) at Stanford University Medical Center Oncology Clinic. Tubes were inverted five times and blood allowed to clot. Tubes were then centrifuged at 1,000 × *g* for 10 min. Serum was extracted and stored at −80 °C until assay.

Benchmark Assays. PSA ELISAs (DKK300; R&D Systems) were conducted on LAPC-4 and DU145 lysates according to manufacturer instructions using a Tecan Infinite microplate reader (Tecan). ELISA calibration standards were run in duplicate; the standard curve was linear in the 1–60 ng mL^{-1} range ($R^2 > 0.99$). Unknown lysate sample were diluted in the range of 20- to 500-fold and run in duplicate, inferred concentrations falling in the linear calibration range were pooled as assay readout. Novex 3–10 IEF gels were run in a Novex Mini-Cell against the Serva protein marker mix according to manufacturer instructions with 1 μg total protein per lane; gels were silver stained with a SilverXpress kit (Invitrogen). Custom slab gels were run on a Mini IEF Cell (Bio-Rad) and were of the same composition as BPMAC- LAVAgels. ε were determined for labeled analytes via fluorescence measurements in loading buffers titrated to pH values in the range of interest and in washout buffer (Fig. S3).

SI Results and Discussion.

Influence of Target Protein Hydrophobicity and Conformation on LAVAgel Capture Efficiency. We found appreciable effects of CE540 labeling on the conformational heterogeneity and capture efficiency of WT GFP. Notably, the ampholyte*, PSA*, and native GFP* η values (at *ca.* 10% each) are all significantly higher than the η of 1.30 ± 0.17% ($n = 44$) measured for unlabeled GFP in the focused state across several chips and experiment days. The hydrophobic structure (5) of CE540 may be the source of this higher η by increasing weak interactions of labeled species with the gel matrix. Further, CE540-labeled WT GFP* exhibits native and denatured protein subpopulations (Fig. S4). During IEF, the native population is characterized by colocalized green (endogenous) and red (CE540) fluorescence (i.e., green+, red+) as anticipated. However, a dominant GFP* population is also observed that lacks any colocalized green signal (i.e., green−, red+). We hypothesize that in this latter population of GFP*, CE540 induces unfolding of GFP sufficient to destroy the green fluorescence of its chromophore. In supporting studies, a microplate experiment showed a sevenfold reduction in green fluorescence of GFP* from that of GFP in an isoelectric ampholyte buffer, providing further evidence for labeling-induced denaturation (Fig. S3). The denatured GFP* segment gives η based on its red CE540 signal of 34.5% (versus 10.1% for the native GFP* segment, see Table S1). This measurement is consistent with the observation that minor conformational increases in solvent-accessible surface area of protein targets produce disproportionately large jumps in diazirine-mediated photolabeling efficiency, suggesting higher protein-label reactivity for looser protein conformations (6). Indeed for labeled, reduced, and denatured proteins in a size-based (SDS-PAGE) assay format to be described in a separate publication, we have observed capture efficiencies of 50–70% in LAVAgels. These observations suggest strong and distinct contributions of protein labeling and conformational disruption on the achievable η.

Benchmark Macroscale IEF Slab Gels. We compared the LAVAgel PSA and GFP readouts to those of a conventional Novex pH 3–10 IEF slab gel (Fig. S5). Slight differences between the LAVAgel and conventional Novex assays of PSA were mitigated using a custom slab gel with the same buffer composition as the LAVAgel. In contrast, the GFP isoforms arising by differential C-terminal proteolytic cleavage (7) exhibited similar behavior in the chip and Novex gels. This comparison study suggests that the isoform pattern of PSA is sensitive to the presence of the solubilizing additives used in LAVAgels (CHAPS, sorbitol, and NDSB-256) that may modulate PSA glycan solvation.

Probe Binding Stoichiometry. Based on antibody probing analyses for purified PSA, the stoichiometry of secondary:primary Ab* binding can be inferred from the ratio of the respective fluorescence traces (Fig. 4*B* and/or Fig. S6). Note that the degrees of labeling of each antibody probe are similar, and that the labeling dye is the same (red Alexa Fluor 568). The binding stoichiometry was determined to be approximately 2.5 across the relevant pH range, exhibiting somewhat higher values at the acidic end of the isoform pattern due to a nonspecific contribution of the secondary Ab* to the assay readout. Remarkably, the observed stoichiometry is in excellent agreement with that of 2.5 determined by Yu et al. using a surface plasmon field-enhanced fluorescence spectroscopy study of polyclonal secondary:primary antibody binding (8).

LAVAgel Assays in Isoform "Affinity Mapping" Mode. To validate the exquisite capability of the LAVAgel assay to measure immunoreagent isoform specificity, we compared the isoform distribution of IEF-focused CE540-labeled PSA* to the fluorescence readout after photoimmobilization and probing with mAb* and pAb* (Fig. S7). Alignment between each pair of fluorescence intensity profiles (PSA*, Ab*) was accomplished by applying a translation inferred from their cross-correlation. The translational shift cor-

rects for the slight drift (*ca.* 190 μm) between imaging of focused PSA* and the photoimmobilization step. The focused PSA* isoform pattern agrees well with that of the probed unlabeled PSA, suggesting little impact of CE540 on the pI values of the native PSA isoforms (compare Fig. S7 *A* and *B* and Fig. 4*A*). Ratiometric comparison of the probed and focused PSA* signals suggests spatially uniform probe layering onto immobilized PSA* across the pH region of interest, for both polyclonal and monoclonal detection antibodies (Fig. S7 *C* and *D*). Some apparent variation across the pH range is induced by diffusional band broadening during photoimmobilization, which has the expected "peak blunting" effect on the probing data. Nonetheless, comparison of the monoclonal and polyclonal probing ratios again reveals a 2.5:1 pAb^*:PSA^* stoichiometry (Fig. S7*E*, assuming a 1:1 stoichiometry inherent in the monoclonal readout with $[Ab^*] \gg K_d$, equilibrium in binding, ref. 9, and negligible PSA "epitope disfigurement" upon immobilization).

Target Antigen Immobilization Kinetics. The reaction between BPMAC and the protein target of interest occurs against a strong background of competing reactions. The bulk of the BPMAC sites are likely to form conjugates with off-target species, namely the ampholytes, gel matrix, sorbitol, NDSB-256, and CHAPS. The combined concentration of these off-target species is >20% wt/vol in the LAVAgel precursor, constituting an approximately 10^6-fold excess over protein targets in the normal device operating regime. Thus, we consider a simple kinetic scheme that characterizes the capture efficiency of a protein target in this regime. Consider parallel irreversible reactions between one reactant (BPMAC, species A) and a set of competing species (species B_i), one of which is the target protein of interest. The reaction scheme is as follows (10):

$$A + B_1 \overset{k_1}{\rightarrow} P_1 \qquad A + B_2 \overset{k_2}{\rightarrow} P_2 \qquad A + B_3 \overset{k_3}{\rightarrow} P_3 \cdots A + B_n \overset{k_n}{\rightarrow} P_n$$

For low capture efficiencies η, it can be assumed that the free species concentrations do not change appreciably from their initial values—i.e., $b_i \sim b_{i,o}$ (lowercase denotes concentration of a species). The rate of disappearance of BPMAC is thus

$$\frac{da}{dt} = -k_T' a,$$

where $k_T' = \sum_{i=1}^{n} k_i' = \sum_{i=1}^{n} b_{i,o} k_i$ is a sum of the pseudo-first-order rate constants k_i' of the competing species.

Integrating this expression gives

$$a = a_o e^{-k_T' t}. \qquad \textbf{[S1]}$$

For generation of a given product P_i

$$\frac{dp_i}{dt} = b_{i,o} k_i a. \qquad \textbf{[S2]}$$

Substituting Eq. **S1** into Eq. **S2** and integrating gives

$$\int_0^{p_i} dp_i = b_{i,o} k_i a_o \int_0^t e^{-k_T' t} dt \Rightarrow p_i = \frac{b_{i,o} k_i a_o}{k_T'} (1 - e^{-k_T' t}). \qquad \textbf{[S3]}$$

This result reveals the unusual property that despite each individual reaction having different pseudo-first-order rate constants ($k_i' = b_{i,o} k_i$) the product generation rates are identical and are characterized by a time constant $\tau = \frac{1}{k_T'} = \frac{1}{\sum_{i=1}^{n} b_{i,o} k_i}$. As we expect $k_T' \gg b_{\text{target},o} k_{\text{target}}$ (subscript "target" denotes the reaction between the protein target of interest and BPMAC)—i.e., that the contribution of k_{target}' to k_T' is small given the vast excess of off-target species in the reaction—we can expect the observed reaction rate to be approximately independent of the target protein concentration. Thus, the observed LAVAgel immobilization time constant is expected to be invariant across the target calibration curve concentration range.

For long reaction times ($t \rightarrow \infty$), from Eq. **S3**

$$p_{\text{target}} = \frac{b_{\text{target},o} k_{\text{target}} a_o}{k_T'} \Rightarrow \eta = \frac{p_{\text{target}}}{b_{\text{target},o}} \times 100 = \frac{k_{\text{target}} a_o}{k_T'} \times 100. \qquad \textbf{[S4]}$$

Again, for k_T' approximately independent of $b_{\text{target},o}$, the LAVAgel capture efficiency is also expected to be independent of $b_{\text{target},o}$ (i.e., constant across the calibration curve). Further, note that increased k_{target}, increased a_o (increased [BPMAC]), or decreased k_T (decreased concentration of competing species and/or rates of competing reactions) all increase η, in accordance with intuition.

Given that the immobilized target concentration is expected to be a constant fraction of the nominal concentration, and that probe saturation of captured target is guaranteed across the calibration curve at equilibrium for $Da \ll 1$ and sufficiently high probe concentration above K_d (see later in this document and ref. 9), we expect a linear calibration relationship in the LAVAgel system, which indeed is observed in the experimental data for PSA.

Finally, the benefit of high immobilization surface area is revealed by considering the volumetric concentration of BPMAC, a_o given a consistent site density $a_{o,s}$ distributed across an immobilization surface with surface area to volume ratio of $\frac{A_s}{V}$:

$$a_o = \frac{a_{o,s} A_s}{V}. \qquad \textbf{[S5]}$$

Substituting Eq. **S5** into Eq. **S4** allows us to determine a ratio of gel to open capillary capture efficiencies:

$$\frac{\eta_{\text{gel}}}{\eta_{\text{cap}}} = \frac{\frac{A_{s,\text{gel}}}{V}}{\frac{A_{s,\text{cap}}}{V}}. \qquad \textbf{[S6]}$$

The gel surface area $A_{s,\text{gel}}$ can be roughly compared to an open capillary $A_{s,\text{cap}}$ by approximating the gel structure to be a bundle of packed cylinders in simple cubic arrangement with radius r_{gel} equal to that of the mean pore radius of 120 nm for a 4%T, 2.6%C gel (11), giving

$$\frac{A_{s,\text{gel}}}{V} \sim \frac{2\pi r_{\text{gel}} l}{(2r_{\text{gel}})^2 l} = \frac{\pi}{2r_{\text{gel}}} \qquad \frac{A_{s,\text{cap}}}{V} \sim \frac{2\pi r_{\text{cap}} l}{\pi r_{\text{cap}}^2 l} = \frac{2}{r_{\text{cap}}}.$$

From Eq. **S6**,

$$\frac{\eta_{\text{gel}}}{\eta_{\text{cap}}} \sim \frac{\pi r_{\text{cap}}}{4 r_{\text{gel}}} = 327$$

with $r_{\text{cap}} = 50$ μm.

We thus expect an approximately two to three order-of-magnitude increase in capture efficiency within the gel matrix as compared to the capillary surface, which is matched well by our experimental observation of an approximately 180-fold improvement in η over that observed by O'Neill et al. (12).

Probe Binding to Immobilized Antigen. Here we compare the timescales of probe mass transfer and binding for a target analyte (P_{target}) immobilized to the wall of an open capillary or to the LAVAgel matrix. In the following analysis, gel and free-solution antibody probe diffusivities of approximately 4.5×10^{-12} and 3.4×10^{-11} $m^2\,s^{-1}$, respectively, are used (see final section). The

capillary tube length y in the open-channel case we take to be the approximate length of an immobilized target peak (*ca.* 100 μm) with tube diameter 100 μm. The surface concentration of target antigen p_{target} is taken to be that resulting from attachment of focused analyte at $\eta = 1\%$ from a 100 nM nominal solution assuming an IEF concentration factor of $\frac{10.4\ \text{mm}}{0.1\ \text{mm}} \sim 100$ onto a surface area arising from the cylindrical pore model already described, which gives $p_{\text{target}} = 7.6 \times 10^{-12}\ \text{mol m}^{-2}$. For equivalence of the two cases, we assume the same p_{target} for the open capillary. The values of $k_{\text{off}} \sim 10^{-3}\ \text{s}^{-1}$ and $k_{\text{on}} \sim 10^{6}\ \text{M}^{-1}\,\text{s}^{-1}$ for Ab-Ag interactions (9, 13).

Consider an immobilized antigen target P_{target} attached to a capillary wall and probed with a detection antibody C to form a stationary complex X:

$$P_{\text{target}} + C \underset{k_{\text{off}}}{\overset{k_{\text{on}}}{\rightleftharpoons}} X.$$

Our interest is in determining when mass transfer limitation of the reaction timescale will occur due to probe depletion near the reaction surface. The rate equation for immunocomplex formation at the surface is

$$\frac{dx}{dt} = k_{\text{on}} c_s p_{\text{target}} - k_{\text{off}} x, \qquad \text{units}: \ \text{mol m}^{-2}\,\text{s}^{-1}, \qquad \textbf{[S7]}$$

where c_s is the surface concentration of probe, which is equal to the bulk probe concentration c_o under conditions of reaction limitation, but is between zero and c_o where mass transfer (by convection at the edge of a boundary layer and diffusion through this layer) to the surface is limiting. Neglecting the "off" term in x, we find the surface flux of probe $\dot{n}_{c_s}$:

$$\dot{n}_{c_s} = -\frac{dx}{dt} = -k_{\text{on}} p_{\text{target}} c_s. \qquad \textbf{[S8]}$$

Here, we consider low probe concentration compared to captured target, which allows the possibility of mass transfer limitation on surface flux of probe. Thus, we lump p_{target} (mol m^{-2}) with k_{on} ($\text{M}^{-1}\,\text{s}^{-1}$) into a pseudo-first-order rate constant k' (standard units of m s^{-1}):

$$\dot{n}_{c_s} = -k' c_s, \qquad k' = k_{\text{on}} p_{\text{target}}. \qquad \textbf{[S9]}$$

This simplified kinetic is sufficient to demonstrate the effect of mass transfer resistance in the surface boundary layer on the apparent rate of immunocomplex formation. For convection, diffusion and reaction under simplifying assumptions that the probe is not depleted at the edge of the boundary layer, and that the probe diffusion profile is at steady state (linear c between c_s and c_o), it can be shown that (9, 14)

$$\dot{n}_{c_s} = -\frac{k' c_o}{1 + \frac{k'}{\beta}}. \qquad \textbf{[S10]}$$

Essentially the probe consumption at the surface depends on a bulk reaction rate $k' c_o$ adjusted by a factor $(1 + \frac{k'}{\beta})$ accounting for mass transfer resistance in the boundary layer, where β is the mass transfer coefficient (ms^{-1}). The dimensionless factor that evaluates the interplay between reaction and mass transfer is the Damkohler number:

$$Da_1 = \frac{k'}{\beta}. \qquad \textbf{[S11]}$$

Thus for $Da_1 \gg 1$, reaction outstrips mass transfer and the system is mass transfer limited with apparent rate $\dot{n}_{c_s} = -\frac{dx}{dt} = -\beta c_o$; whereas for $Da_1 \ll 1$, mass transfer outstrips reaction and the system is reaction limited with apparent rate $\dot{n}_{c_s} = -\frac{dx}{dt} = -k' c_o$.

The mass transfer coefficient β is a component of the Sherwood number Sh (a mass transport analog of the Nusselt number in heat transfer), which can be estimated from empirical relations determined for different flow properties and interface geometries (15).

$$Sh = \frac{\beta l}{D} = \frac{\text{mass transfer velocity}}{\text{diffusion velocity}}, \qquad \textbf{[S12]}$$

where l is a characteristic length in the system.

For the open capillary case, an accurate (within *ca.* 1%) relationship for laminar flow in a cylindrical tube is readily available (15):

$$Sh = \frac{\beta d}{D} = 1.62\left(\frac{d^2 u}{yD}\right)^{\frac{1}{3}}, \qquad \textbf{[S13]}$$

where d is the tube diameter, y the tube length (length of the reaction zone in our case), u the average velocity in the tube, and D the diffusivity of the probe in free solution.

Eqs. **S11** and **S13** give Da_1 for probe flowrates greater than $u \sim 1\ \text{mm s}^{-1}$. Further decreases in Da_1 occur relatively "slowly" with increases in u due to the cube root dependence of Sh on u. However, given that $\eta \sim 0.01\%$ would be much more reasonable in the open capillary case, we quickly find $Da_1 \ll 1$, and thus that the probing step is reaction rather than mass transfer limited.

For LAVAgel probing, the target antigen is distributed throughout the channel volume, suggesting that probe driven through the gel pores reacts with captured antigen in a homogeneous fashion (i.e., no boundary layer resistance exists). An alternative Damkohler number has been posited for such electrophoretic "band crossing" reactions (16):

$$Da_2 = \frac{t_{\text{cross}}}{\tau_R}, \qquad \textbf{[S14]}$$

where $t_{\text{cross}} = \frac{w}{u_{\text{rel}}}$ is the time required for the probe front to sweep through the captured band, which is approximately 2 s given an observed probe velocity of $u_{\text{rel}} \sim 50\ \text{μm s}^{-1}$ in LAVAgels and a target band width $w = 100$ μm. We also expect reaction-limited conditions ($Da_2 \ll 1$) in this framework given the experimental observation that $t_{\text{cross}} \ll \tau_R$ (Fig. 2*D*).

To summarize, we expect $Da_{1,2} \ll 1$ such that the relevant probe transport timescale is always much smaller than the reaction timescale (i.e., mass transfer faster than reaction). With this result, we recast the binding reaction at the surface to focus on depletion of captured target as it is occupied by relatively unconstrained delivery of probe:

$$\frac{dx}{dt} = k_{\text{on}} c_s p_{\text{target}} - k_{\text{off}} x. \qquad \textbf{[S15]}$$

This equation is identical to Eq. **S7**, but here we take $c_s \sim c_o$ and $p_{\text{target}} = (p_{\text{target,total}} - x)$ where $p_{\text{target,total}}$ is the total concentration of immobilized target and solve to find (9)

$$\frac{x(t)}{p_{\text{target,total}}} = \frac{c_o / K_{\text{d}}}{1 + c_o / K_{\text{d}}}\left(1 - e^{-(k_{\text{on}} c_o + k_{\text{off}})t}\right) \quad \text{for } Da_{1,2} \ll 1, \qquad \textbf{[S16]}$$

where $K_{\text{d}} = \frac{k_{\text{off}}}{k_{\text{on}}}$ is the equilibrium dissociation constant for the Ab-Ag interaction.

We choose the bulk probe antibody concentration c_o to be in large excess compared to K_{d} at $c_o > 100$ nM, giving $\tau_R \lesssim \frac{1}{k_{\text{on}} c_o} = 10$ s (note that in hindsight, $t_{\text{cross}} \ll \tau_R$, as observed

experimentally), and at equilibrium $\frac{x(t)}{p_{\text{target,total}}} = \frac{c_o/K_d}{1+c_o/K_d} \sim 1$ (i.e., probe binding saturates captured target). The fact that the observed value of τ_R is instead on the order of 5 min in LAVAgels (Fig. 2*D*) perhaps points to the fact that the kinetic "on" and "off" rates are distorted in the gel environment (likely both will be decreased due to the presence of the gel matrix, as is currently under study by our group; ref. 2). In any case, values for k_{on} and k_{off} can vary considerably depending on the antibody-antigen pair used (13), so the 10-s result can be viewed as being in the expected range given the assumptions made.

Determination of Free-Solution and In-Gel Diffusivities. The diffusion coefficient for GFP in 4%T, 2.6%C polyacrylamide gel was determined by defocusing to be 2.05×10^{-7} cm^2 s^{-1} (Fig. 3*A*). The diffusion coefficient for a given protein in a polyacrylamide matrix can be estimated via an adjusted Stokes–Einstein diffusivity (17, 18):

$$r_H = 0.595(M_M)^{0.427} \quad \textbf{[S17]}$$

$$D = \frac{k_B T}{6\pi\mu r_H} e^{-k_c r_H \phi^{0.75}}, \quad \textbf{[S18]}$$

where r_H is the protein hydrodynamic radius, M_M the protein molecular mass in kilodaltons, k_B is Boltzmann's constant, T temperature, μ the viscosity of the medium ($\mu \sim 1.26 \times 10^{-3}$ Pa·s for a 10% sorbitol solution; ref. 19), $k_c = 0.45$ angstrom^{-1}, and ϕ the polymer volume fraction.

This relationship gives a diffusivity of GFP in 4%T, 2.6%C polyacrylamide gel of approximately 2.5×10^{-7} cm^2 s^{-1}, which is within 20% of the value measured by defocusing (2.05×10^{-7} cm^2 s^{-1}). Thus, the diffusivity for a probe antibody can be confidently estimated by similar means to be approximately 4.5×10^{-8} cm^2 s^{-1} in the gel and approximately 3.4×10^{-7} cm^2 s^{-1} in free solution.

1. Righetti PG (1983) *Isoelectric Focusing: Theory, Methodology and Applications* (Elsevier, New York).
2. Hughes AJ, Herr AE (2010) Quantitative enzyme activity determination with zeptomole sensitivity by microfluidic gradient-gel zymography. *Anal Chem* 82:3803–3811.
3. Stone KR, Mickey DD, Wunderli H, Mickey GH, Paulson DF (1978) Isolation of a human prostate carcinoma cell line (DU 145). *Int J Cancer* 21:274–281.
4. Klein KA, et al. (1997) Progression of metastatic human prostate cancer to androgen independence in immunodeficient SCID mice. *Nat Med* 3:402–408.
5. Craig DB, Wetzl BK, Duerkop A, Wolfbeis OS (2005) Determination of picomolar concentrations of proteins using novel amino reactive chameleon labels and capillary electrophoresis laser-induced fluorescence detection. *Electrophoresis* 26:2208–2213.
6. Jumper CC, Schriemer DC (2011) Mass spectrometry of laser-initiated carbene reactions for protein topographic analysis. *Anal Chem* 83:2913–2920.
7. Ward WW (2006) Biochemical and Physical Properties of Green Fluorescent Protein. *Green Fluorescent Protein: Properties, Applications and Protocols*, eds Chalfie M, Kain SR (Wiley, Hoboken, NJ).
8. Yu F, Yao D, Knoll W (2003) Surface plasmon field-enhanced fluorescence spectroscopy studies of the interaction between an antibody and its surface-coupled antigen. *Anal Chem* 75:2610–2617.
9. Squires TM, Messinger RJ, Manalis SR (2008) Making it stick: Convection, reaction and diffusion in surface-based biosensors. *Nat Biotechnol* 26:417–426.
10. Steinfeld JI, Francisco JS, Hase WL (1989) *Chemical Kinetics and Dynamics* (Prentice Hall, Englewood Cliffs, NJ).
11. Holmes DL, Stellwagen NC (1991) Estimation of polyacrylamide gel pore size from Ferguson plots of linear DNA fragments II. Comparison of gels with different cross-linker concentrations, added agarose and added linear polyacrylamide. *Electrophoresis* 12:612–619.
12. O'Neill RA, et al. (2006) Isoelectric focusing technology quantifies protein signaling in 25 cells. *Proc Natl Acad Sci USA* 103:16153–16158.
13. Tia SQ, He M, Kim D, Herr AE (2011) Multianalyte on-chip native Western blotting. *Anal Chem* 83:3581–3588.
14. Baehr HD, Stephan K (2006) *Heat and Mass Transfer* (Springer, Berlin), 2nd Ed.
15. Cussler EL (1997) *Diffusion: Mass Transfer in Fluid Systems* (Cambridge Univ Press, Cambridge, UK), 2nd Ed.
16. Matta A, et al. (2004) Computational study of band-crossing reactions. *J Microelectromech Syst* 13:310–322.
17. Wei Y, Wesson PJ, Kourkine I, Grzybowski BA (2010) Measurement of protein-ligand binding constants from reaction-diffusion concentration profiles. *Anal Chem* 82:8780–8784.
18. Konzak S, Thies E, Marx A, Mandelkow EM, Mandelkow E (2007) Swimming against the tide: Mobility of the microtubule-associated protein tau in neurons. *J Neurosci* 27:9916–9927.
19. Liu Y, Shi M, Cao R, Zhang Y, Hu Y (2007) Densities and viscosities of the quaternary system mannitol-sorbitol-D-glucose-H2O and its ternary subsystems at 298.15K*. *Chin J Chem Eng* 15:703–709.

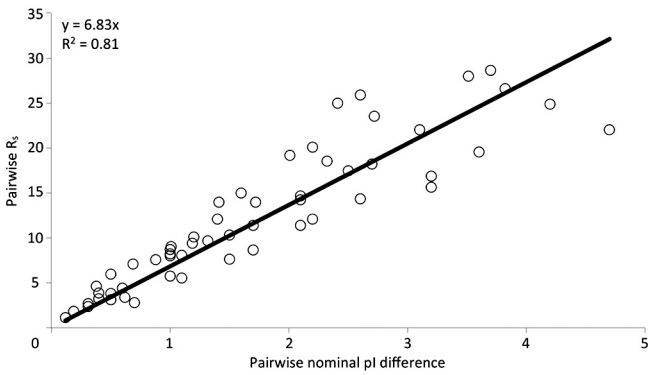

Fig. S1. Separation resolution of analyte pairs under focusing conditions for the 8 pI markers and 3 GFP isoforms presented in Fig. 2*B* (55 total comparisons). A threshold of $R_s = 1$ yields a minimum separable pI difference of 0.15 via linear regression.

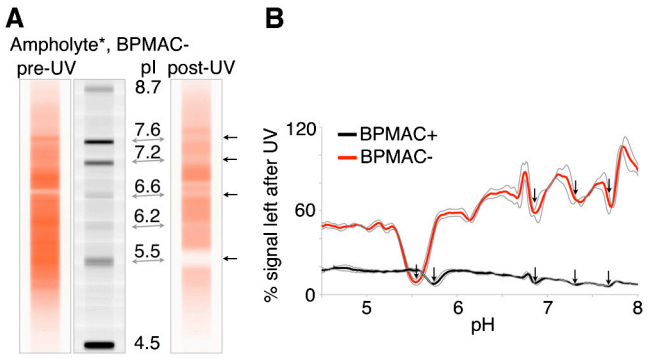

Fig. S2. Colocalized ampholyte* species and pI markers yields enhanced photobleaching. (*A*) Effect of 10 s flood UV exposure on ampholyte* profile in the focused state prior to washout. pI markers exacerbate local ampholyte* bleaching (gray and black arrows). (*B*) Ampholyte* signal retained after UV exposure. Troughs in pI marker regions are marked by black arrows. Note, higher overall bleaching occurs in BPMAC+ LAVAgels, presumably due to side reactions between ampholyte* radicals and other reactive species generated upon BPMAC photoactivation (1).

1. Gilbert A, Baggott J (1991) *Essentials of Molecular Photochemistry* (Blackwell, Cambridge, MA).

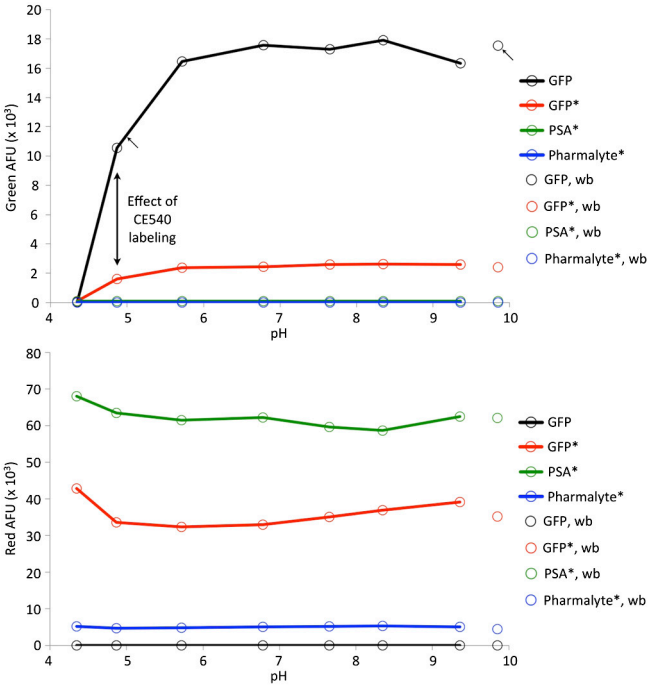

Fig. S3. Microplate experiments reveal denaturing effect of GFP labeling and allow extraction of η. (*Upper*) Solid lines are microplate green fluorescence data for analytes (1 μM each) in 50 μL aliquots of loading buffers titrated to the measured pH values shown with 2M HCl or NaOH. Data points at pH 9.9 are for washout buffer (wb) samples (AFU, arbitrary fluorescence units). ε for GFP is approximated via the ratio of fluorescence values at the points indicated by short arrows. The strong pH effect of GFP's fluorescence in the vicinity of its pI is well known in the literature (7). (*Lower*) Corresponding red fluorescence values for each analyte, note the negligible dependence of CE540 fluorescence on pH for all labeled species.

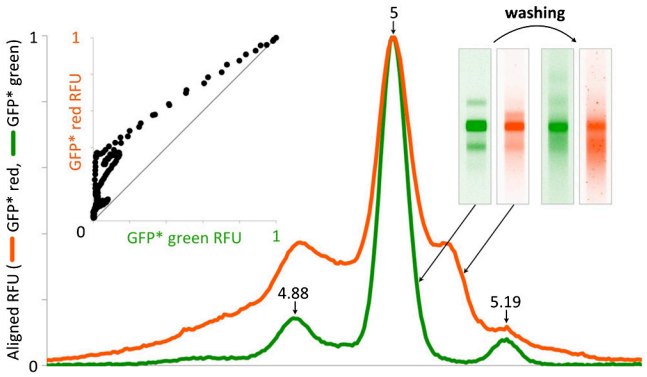

Fig. S4. CE540-labeled GFP exists as native (green+, red+) and denatured (green−, red+) subpopulations. Aligned relative fluorescence data from sequential imaging on green and red spectral channels for GFP* focused at 300 V cm^{-1} in a single LAVAgel (RFU, relative fluorescence units; nominal $[GFP^*] = 617$ nM). The red fluorescence readout is dominated by the denatured population, presenting as a diffuse set of bands with rough correspondence to those of the native GFP* population (green fluorescence readout). The canonical three-band structure observed for the native GFP* population is very similar to that of unlabeled GFP (Fig. 2*B*).

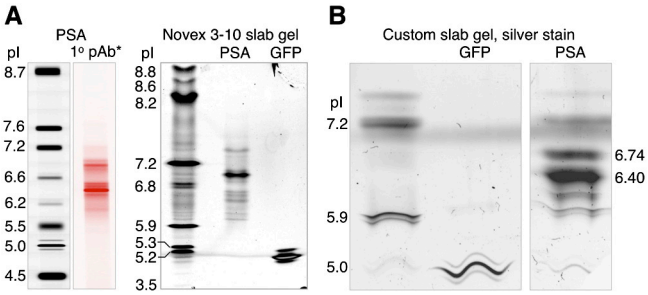

Fig. S5. LAVAgel and companion slab-gel IEF assays. (*A*) Comparison of purified PSA and GFP readouts in LAVAgel to Novex slab gel (LAVAgel GFP visible in pI marker set). (*B*) PSA isoform pattern in custom slab gel agrees with major band assignments in LAVAgels (gel buffer compositions here were identical to those in LAVAgels).

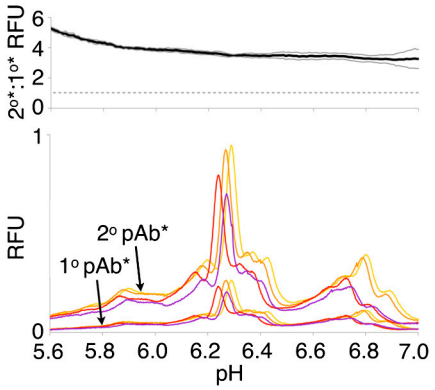

Fig. S6. Inference of probe stoichiometry for purified PSA. (*Lower*) Comparison of signal after 1° and 2° probing for 500 nM PSA (RFU, relative fluorescence units). (*Upper*) Signal amplification ratio 2°:1° (dotted line marks baseline of nil 2° signal at 2°:1° = 1, gray envelope is ±SD, $n = 4$).

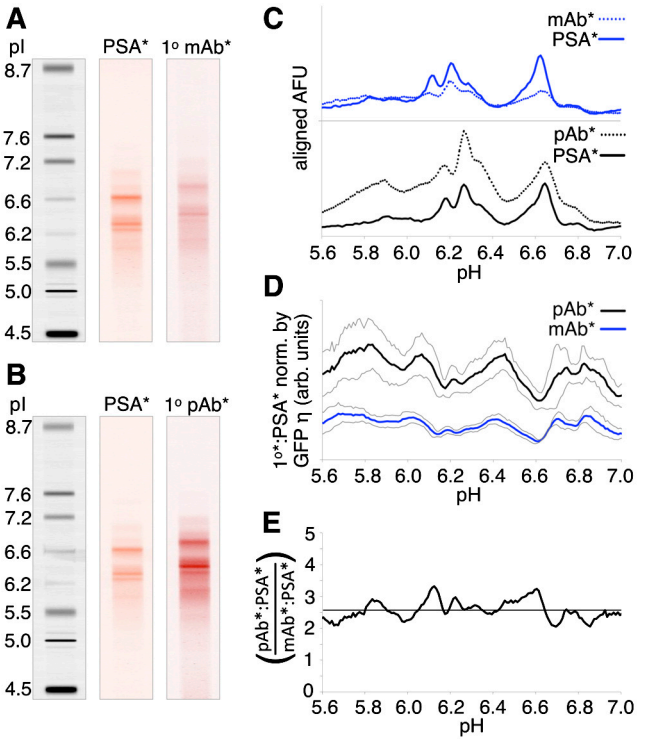

Fig. S7. LAVAgel assays in recognition mapping mode for isoform-resolution probe screening. (*A*) CE540-labeled PSA* in focused and probed states for monoclonal and (*B*) polyclonal Ab* (all gel images adjusted for identical contrast, $[\text{PSA}^*] = 500$ nM, $[\text{mAb}^*, \text{pAb}^*] = 1$ μM). Electrophoretically washed PSA* data showed negligible contribution to probe signals by immobilized PSA* detected on the same spectral channel. (*C*) 1° Ab* readouts aligned to corresponding focused PSA* traces from *A* and *B* (AFU, arbitrary fluorescence units). (*D*) Probed:focused signal ratios adjusted by GFP capture efficiency (gray envelopes are ±SD, $n = 8$ for each of mAb* and pAb* sets). (*E*) Ratio of pAb*:mAb* data from (*D*).

Table S1. LAVAgel capture efficiencies η (%) under focusing conditions

Target	pH	η_{green}	η_{red}
GFP	*ca.* 5.2	1.30 ± 0.17 ($n = 44$)	—
GFP*	*ca.* 5.2	10.1 ± 1.91 ($n = 8$)	34.5 ± 3.04 ($n = 8$)
PSA*	*ca.* 6.5	—	9.92 ± 0.86 ($n = 3$)
Pharmalyte 3–10*	5.0	—	7.17 ± 1.95 ($n = 4$)
	7.5	—	13.3 ± 1.70 ($n = 4$)

Red CE540-labeling indicated by "*", fluorescence emission channel used to determine η denoted by "green" and "red" in subscripts.